Monolithic integration of fine cylindrical glass microcapillaries on silicon for electrophoretic separation of biomolecules

Zhen Cao, Kangning Ren, Hongkai Wu, and Levent Yobas

Additional information on Biomicrofluidics

Journal Homepage: http://bmf.aip.org/
Journal Information: http://bmf.aip.org/about/about_the_journal
Top downloads: http://bmf.aip.org/features/most_downloaded
Information for Authors: http://bmf.aip.org/authors

Monolithic integration of fine cylindrical glass microcapillaries on silicon for electrophoretic separation of biomolecules

Zhen Cao,[1] Kangning Ren,[2] Hongkai Wu,[2,3] and Levent Yobas[1,3,a]

[1]*Department of Electronic and Computer Engineering, Hong Kong University of Science and Technology, Clear Water Bay, Kowloon, Hong Kong*
[2]*Department of Chemistry, Hong Kong University of Science and Technology, Clear Water Bay, Kowloon, Hong Kong*
[3]*Division of Biomedical Engineering, Hong Kong University of Science and Technology, Clear Water Bay, Kowloon, Hong Kong*

We demonstrate monolithic integration of fine cylindrical glass microcapillaries (diameter $\sim 1\,\mu$m) on silicon and evaluate their performance for electrophoretic separation of biomolecules. Such microcapillaries are achieved through thermal reflow of a glass layer on microstructured silicon whereby slender voids are moulded into cylindrical tubes. The process allows self-enclosed microcapillaries with a uniform profile. A simplified method is also described to integrate the microcapillaries with a sample-injection cross without the requirement of glass etching. The 10-mm-long microcapillaries sustain field intensities up to $90\,$kV/m and limit the temperature excursions due to Joule heating to a few degrees Celsius only. © 2012 American Institute of Physics. [http://dx.doi.org/10.1063/1.4739075]

I. INTRODUCTION

Over the years, microcapillary electrophoresis (μCE)[1] has been evolved with numerous innovations addressing a particular aspect of the original concept such as microfabrication,[2] sample injection,[3] separation speed,[4] separation efficiency,[5] integrated sample preparation,[6] and analyte detection.[7] Substantial progress has been made towards the commercialization of the technology for laboratory and point-of-care use.[8] Yet, few important issues have remained to be addressed: (1) excessive Joule heating through the capillary; (2) non-uniform zeta potential (ζ) on the capillary walls and the accompanying unstable electroosmotic flow (EOF); (3) depletion of analytes to the capillary walls due to analyte-surface interactions; and (4) challenges with the fabrication techniques such as etching, alignment, and substrate bonding to integrate the capillary.

Joule heating arises from resistive losses through the ionic buffer and prevents large enough field strengths to be applied to resolve multiple bands. Band broadening and analyte dispersion adversely affect the separation quality and get further exacerbated by excessive heating and thermal gradients. CE, particularly μCE, owing to a high surface-to-volume ratio (SVR) of a small capillary or a planar microchannel, removes heat much quicker than the traditional slab-gel electrophoresis, and tolerates much larger field strengths, thereby achieving a higher separation speed and resolution.[9] Still, the experiments with the μCE devices suggest that the heat removal efficiency may not be adequate to avoid performance degradation at higher voltages.[10–12] Some of these devices make use of glass or polymer substrates, which may not be that effective in heat removal. To address the issue, researchers have taken a step towards reducing the capillary/channel diameter and thereby further increasing SVR. Sun *et al.* used a photonic crystal fiber (PCF), a bundle of fused-silica capillaries, each with a diameter $3.7\,\mu$m.[13] By directly embedding a short PCF segment in a separation microchannel engraved in a polymer substrate, they managed to demonstrate improved heat dissipation and separation performance as compared to a typical micromachined all-glass μCE device.

---

[a]Author to whom correspondence should be addressed. Electronic mail: eelyobas@ust.hk. Tel.: (+852) 2358–7068.

6, 036501-1

Surface properties of the capillary or microchannel walls are of utmost importance for reliable electrophoretic separation. Particularly, the capillaries defined in polymeric substrates such as poly(dimethylsiloxane) (PDMS), poly(methyl methacrylate) (PMMA), and poly(carbonate) (PC) possess a hydrophobic surface that could lead to sample loss by analyte adsorption. Moreover, non-uniform adsorption of species on the capillary wall alters the ζ potential along the capillary, creating an unstable EOF.[14] To alleviate these concerns, researchers have applied various surface modification strategies such as dynamic coating of the walls with suitable modifiers dissolved in the running buffer,[15] surface-adsorbed coating with a glass-like film,[16] and surface-covalent coating by treating the walls with plasma.[17] These approaches all mitigate the surface-related issues but at the expense of reproducibility and efficiency. Alternatively, Dimov *et al.* proposed a hybrid device whereby the separation channel is defined by a standard fused-silica capillary segment embedded in a PDMS chip which contains sample-injection microfluidics.[18]

Surface chemistries for the traditional CE capillaries are readily available and make the μCE devices fabricated out of silica-based substrates such as silicon,[19] glass,[20] and quartz[21] attractive. Though, creating well-defined capillaries in these materials, apart from silicon, is problematic. Particularly, wet etching glass leaves behind a poor surface finish.[22] Additionally, residual stresses in glass cause defects during etching and have to be released through thermal or chemical pretreatment.[20,23] Plasma or dry etching of glass suffers from low etch rate and selectivity, and rough surface finish.[24] Non-uniformities on the etched capillary walls become potential adsorption sites and may perturb plug flow with distorted slip velocity and induced local pressure fields.[25] Moreover, a cover plate has to be carefully aligned and secured on the etched capillaries. The bonding can be extremely sensitive to the presence of a particulate at the surface, demanding rigorous cleaning steps.[20,21] Furthermore, the capillary walls defined by separate substrates could lead to plug dispersion unless their ζ potentials are perfectly matched.[26] To minimize dispersion and thereby achieve more efficient separation, it is desired to have a monolithic capillary surrounded by a single substrate rather than a pair whether be it homogenous or hybrid (e.g., glass/polymer).[27,28]

The work presented here may overcome some of these limitations with the μCE devices by introducing monolithically integrated self-sealed fine cylindrical glass microcapillaries on silicon.[29] Previously, we demonstrated such in-plane microcapillaries for electrophysiology on chip and employed their substantially round and smooth opening (diameter $<2\,\mu$m) to dock and monitor individual cells and their ionic activity (i.e., whole-cell patch clamping).[30–32] However, the earlier microcapillaries had to be made extremely short ($<50\,\mu$m) to limit their access resistance and thus the recording noise. In comparison, much longer microcapillaries are needed for the electrophoretic separation of molecules. Here, we show that these microcapillaries can be made at a greater length scale while preserving their round and uniform cross-sectional profile along the capillary length. Still leveraging on the same fabrication principle, thermal reflow of a glass layer on a structured silicon and the subsequent void transformation within narrow trenches [Figs. 1(a) and 1(b)], we integrate self-sealed round microcapillaries with a sample-injection cross [Fig. 1(c)] and investigate their performance on the electrophoretic separation of
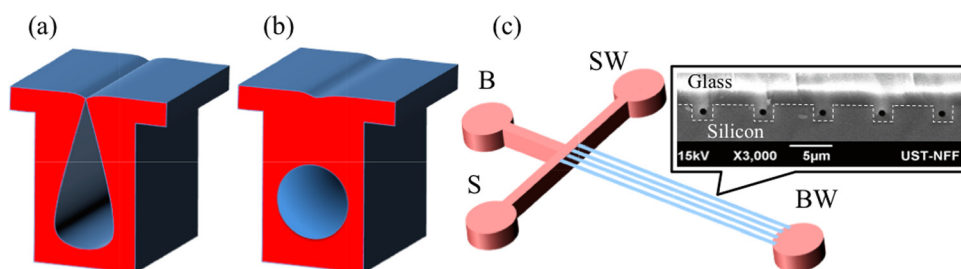

FIG. 1. Conceptual illustration of the self-sealed glass in-plane microcapillaries with a round cross-sectional profile on silicon and their integration with a sample-injection cross in a μCE: (a) a void (keyhole) being trapped inside a rectangular trench due to non-conformal deposition of the glass filling; (b) the same void after being transformed into a round glass capillary via thermal reflow process; (c) an array of self-sealed glass microcapillaries integrated with the classical design of a sample-injection cross. The reservoirs: buffer (B), buffer waste (BW), sample (S), and sample waste (SW).

three amino acids. We also report on an improvement in the fabrication process whereby the cumbersome step of etching glass layer is eliminated entirely.

II. METHOD

A. Reagents and buffers

Running buffer, sodium tetraborate decahydrate (borate), was prepared in deionized (DI) water at a concentration of 10 mM and filtered through a membrane with cut-off size 0.22 μm (Millipore). Three amino acids (Sigma-Aldrich), Glycine (Gly), Serine (Ser), and Glutamine (Gln) were individually dissolved in the running buffer to a concentration of 1 mM (*p*H 9.2) and labeled with fluoresceine-5-isothiocyanate (FITC) by mixing at 100:1 (v/v) and incubating in dark overnight. FITC solution was prepared at a concentration of 1 mM by dissolving 10 mg FITC (Molecular Probes) in 25 ml acetone. Before the analyses, amino acids were mixed at 1:1:1 (v/v/v) (*p*H 10.2).

B. Device fabrication

The fabrication of the cylindrical glass microcapillaries was previously detailed.[29–32] It was further modified here to simplify the overall process and enhance their dielectric breakdown against high voltages. The fabrication takes advantage of the so-called "keyhole" formation, a well-known problem in the fabrication of integrated circuits. The keyhole is an undesired void being trapped in an isolation trench due to non-conformal deposition of the dielectric filling. Such structure can then be turned into a round tunnel or a microcapillary under a thermal reflow of the filling material. The final size of the microcapillary can be controlled by mainly the aspect ratio of the trench, the filling material thickness to some extent, and reflow temperature and duration.[29] Glass microcapillaries (diameter $<2\,\mu$m) were fabricated here on p-type (100)-oriented silicon wafers (diameter 100 mm). Distinct from our earlier process, the wafers were pre-structured with a dual step profile as schematically described in Fig. 2(a). Each shallow step (3.5 μm deep) formed a narrow trench (3 μm wide), in which a self-sealed glass microcapillary would be molded, while a deeper step (25 μm deep) defined the sample-injection cross (10−100 μm wide) and the inlet/outlet reservoirs (diameter 1 mm). Most of the trenches adopted a diverging layout towards their ends expanding and terminating at a larger width than their nominal width of 3 μm.

Briefly, a thin-film silicon dioxide (1 μm thick) was deposited on the wafers and patterned such that it exposes the substrate at the sites to be etched [mask I in Fig. 2(b)]. To attain a dual-step profile, a photoresist layer was spun on the oxide layer and then patterned with a
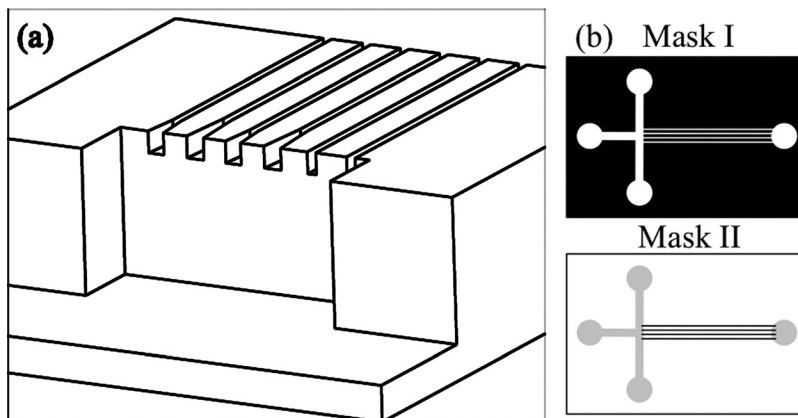

FIG. 2. Schematic illustrations for microfabrication: (a) isometric view of a pre-structured silicon substrate with a dual step profile prior to the deposition and thermal reflow of the glass filling layer and (b) the mask layouts used in the integration of the microcapillaries (the shaded regions in mask II are drawn only to show the mask-to-mask alignment).

layout masking the trench locations (mask II). Through the photoresist and oxide patterns, the wafers were dry etched in a deep reactive ion etching (DRIE) chamber (STS) for 20 min creating the microchannels and the reservoirs. Subsequently, the photoresist pattern was stripped off and the DRIE process continued with the oxide pattern for another 3 min, forming the shallow trenches while deepening the microchannels and the reservoirs. After stripping off the etch mask, the wafers were sent to an oxidation furnace to grow a thermal oxide film (thickness range $0.5-1\,\mu m$). Subsequently, phosphosilicate glass (PSG) was deposited through a chemical vapor deposition (180 mTorr, 420 °C) at a thickness of $5\,\mu m$ trapping a triangular void within each trench as a result of the non-conformal deposition profile. In the final step, the wafers were annealed at 1000 °C for 60 min to allow for the glass filling within the trenches to reflow, rounding off the voids into cylindrical capillaries.

C. Packaging and loading the device

The glass microcapillaries, since they are self-sealed structures buried in the glass layer, do not require a capping layer and yet the sample-injection cross does need a capping. For convenience, polydimethylsiloxane (PDMS; Dow Corning 184) was molded into a single plain slab ($\sim$5 mm thick), which was then bored with four inlet/outlet holes (diameter 3 mm) overlapping the reservoirs of the silicon device under test. The PDMS slab was then aligned and permanently bonded over the device after activating their surfaces through oxygen plasma (29.6 W for 1 min, Harrick Plasma). Each device, as soon as bonded, was filled with the prepared solutions. A FITC solution (0.1 mM) was pipetted into reservoirs S, sample waste (SW), and B (as labeled in Fig. 1) and the microcapillaries were inspected under an epi-fluorescence microscope for a visual assessment. For an electrophoretic separation of the amino acids, the subsequent devices were filled with the running buffer by pipetting the buffer first into reservoirs SW and B, and then BW, all in equal volume (20 μl each). Reservoir S was then loaded with a sample mixture (20 μl).

D. Injection, separation, and detection

The device under test was placed on the stage of an epi-fluorescence microscope (FN1; Nikon, Japan) equipped with a halogen lamp, a mercury lamp (100 W), and the filter cube for FITC detection (Ex/Em 492/520 nm). Images were captured and stored in a computer through a CCD camera (RT3 Mono; SPOT) mounted on the microscope. For the electrophoretic separation, platinum electrodes (Leego Precision Alloy, China) were immersed into the reservoirs and connected to a high-voltage power supply (Tianjin Dongwen Co., Ltd, China) controlled through LABVIEW (National Instruments). The following voltage protocol was applied during sample loading: 500 V to reservoir S, 450 V to B, and 500 V to BW, while grounding SW for about 25 s. During separation, reservoir BW was held at ground potential while having reservoir B held at 300 V and both S and SW at 100 V (pullback) for 40 s. For laser-induced fluorescence detection, a laser beam of 473 nm was directed into the microscope from a diode-pumped solid-state laser (LSR473NL, Lasever Inc.) replacing the halogen lamp-house. The laser beam was aligned and focused on the microcapillaries 1 mm from reservoir BW through a 10$\times$ objective (NA 0.3). The time-series images collected were analyzed by an image processing software (ImageJ; NIH, Bethesda) to generate electropherograms by extracting and plotting fluorescence intensities from the region of interest (ROI $\sim 2\,\mu m$ by $2\,\mu m$).

III. RESULTS

A. Microcapillary structures

Figs. 3(a) and 3(b) show scanning electron microscopy (SEM) images of the sample-injection cross from a representative silicon device prior to the deposition and reflow of the glass layer. The images reveal the dual step profile where the sample-injection channel 25 μm deep meets the trenches 3.5 μm deep. A repeating pattern of ten trenches (total 20) is accommodated in this particular design with all the trenches being identical except that they terminate at
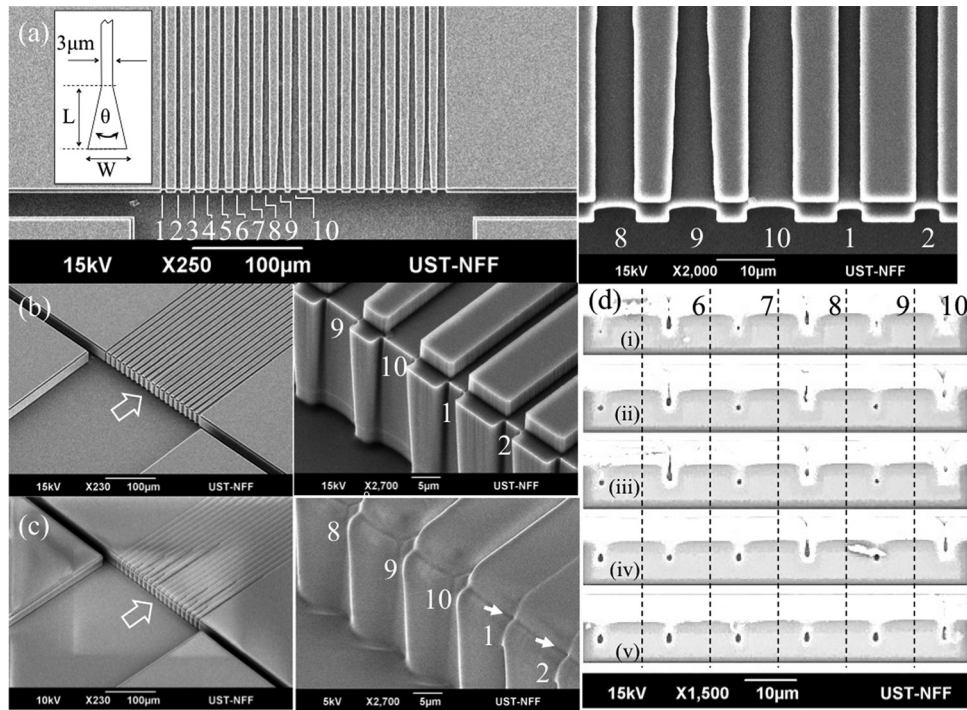
FIG. 3. SEM images of the sample-injection cross from a representative device: (a) plane and (b) isometric views taken prior to the deposition of the glass filling; (c) isometric views after the deposition and thermal reflow of the glass filling. The outlined arrows in (b) and (c) mark the sites for the close-up shots. The inset in (a) is a schematic description of a trench termination layout showing critical dimensions (Table I). The numerals (1–10) identify the microcapillary designs (Table I). The solid arrows in (c) point at the sites where 1 and 2 appear distinct from 8, 9, and 10 and thus their access ports probably did not emerge. (d) SEM cross-sectional images of 5–10 taken from the step at a distance of (i) 30 μm, (ii) 60 μm, (iii) 120 μm, (iv) 180 μm, and (v) 240 μm showing the evolution of the microcapillary access ports.

a different width. A layout of trench termination is described by a simple schematic indicating the critical dimensions in Fig. 3(a) (the inset). The values assigned to these dimensions are listed for each trench in Table I. Trenches 1 and 2 both maintain their uniform 3 μm width throughout their length while the rest terminate at a larger width gradually expanding from 3 μm following a fixed angle (Table I). As can be noticed from the image, the width of termination increases from 4 μm to 7 μm with the trench number. The angle of expansion θ is kept below 1° for the even numbered trenches while at 1° < θ < 5° for those odd numbered.

Fig. 3(c) reveals the same structure following the deposition and reflow of the glass layer. This profile expectedly differs from our previous devices in which the round cross-sectional profile of a microcapillary is intentionally exposed and directly accessible upon dry etching glass/silicon. Etching is avoided here particularly because it would expose the underneath silicon which had to be re-insulated again adequately by either thermal oxidation or an additional dielectric layer deposition to withstand a high driving voltage. Oxidizing silicon, however, could cause the existing glass layer to further reflow and collapse under high temperatures while the additional dielectric deposition could seal off any fluidic access to the microcapillaries. Thus, revising the process as prescribed here would allow for a better insulation of the pre-structured silicon substrate through a

TABLE I. List of values assigned to the critical dimensions of the layout defined in Fig. 3(a) (inset).

Trench No.	3	4	5	6	7	8	9	10
W (μm)	4	4	5	5	6	6	7	7
L (μm)	50	100	50	150	50	200	50	250
θ (deg)	1.2	0.6	2.3	0.8	3.4	0.9	4.6	0.9

composite layer of the thermal-oxide film (1–2 μm thick) and the subsequent glass layer (5 μm thick). Since the etching is no longer available to create access ports to the microcapillaries, the trenches are designed here with both ends open so as to prevent them from getting completely sealed off, as was the case with our previously reported devices. Anticipating that this alone may not be sufficient to develop well-defined access ports to the microcapillaries, trench designs with gradually widening ends were also included. The SEM image [Fig. 3(c)] supports this claim as trenches 1 and 2 (without sufficiently wide ends) are shown completely sealed off from the above as well as from the side (the solid arrows). Meanwhile, those terminating at a width $\geq 5 \mu$m (trenches 5−10) did not get immediately sealed off right at the step edge but rather remained open until their width shrinks below 5 μm. Still, from the shown image, it is unclear whether these openings are indeed extensions of the microcapillaries buried within the trenches. This will be clarified through a simple fluidic test below.

To investigate the evolving access ports, cross-sectional SEM images were taken from trenches 5–10 along their length at $\leq 60 \mu$m intervals. Fig. 3(d) shows these images and suggests that the openings on the surface could indeed lead to the buried microcapillaries. Several interesting points emerge from the images are worthy of a note. First, a surface opening with a large angle of expansion (trenches 5, 7, and 9) quickly converges into a self-sealed cylindrical microcapillary over a short distance $\sim 30 \mu$m in the case of (i) whereas an opening with a smaller angle (trenches 6, 8, and 10) may require a longer distance to do so, 180 μm in (iv) or 240 μm in (v). Second and perhaps more puzzling, the wider a trench gets the smaller the diameter of a microcapillary becomes, which can be verified through a comparison of images between (i) and (iv), particularly for those with a large angle of expansion (5, 7, and 9). This suggests that fabrication of submicron cylindrical glass capillaries through our method should be viable without the requirement of a high-resolution advanced lithography. Typical diameters along the uniform trench width are about 900 nm according to the direct measurements on the SEM images of the cross-sectioned devices. The device-to-device and run-to-run variations are in agreement with our earlier studies[29–32] and remain <10%. These variations are largely attributed to the deviations in the trench aspect ratio as a result of the dry etching process.

B. Fluidic access

Fluidic access to the microcapillaries was verified through a FITC solution loaded into the injection cross and allowed to flow into the round microcapillaries under the capillarity [Fig. 4(a)]. In many of the devices tested, microcapillaries 7–10 were found completely filled with the FITC solution while microcapillaries 5 and 6 were filled only on rare cases. Microcapillaries 1–4, as their termination width falls below 5 μm, were found either completely blank or filled only partially by a short segment ($<50 \mu$m) from the injection cross junction. These results suggest that, for the given process conditions (e.g., glass layer thickness), there exists a minimum width of termination that needs to be fulfilled to ensure fluidic access to the microcapillaries. The results also suggest that the width of termination could play a more dominant role than the angle of expansion. For instance, trench 5 as compared to trench 8 has a larger angle of expansion ($2.3° > 0.9°$) and yet cannot be always filled, as its termination width is slightly narrower (5 μm < 6 μm). To test whether the filling can be facilitated by suction, reservoir BW was connected to a vacuum pump with the remaining reservoirs left open to the atmosphere. This, however, did only help for microcapillaries 5 and 6 occasionally after >30 min suction. Thus, the electrophoretic separation results below are from microcapillaries 6–10.

C. Breakdown voltage

Thus far, silicon has been mostly avoided as a substrate material for μCE partly because it requires a dielectric insulation. The insulation layers are prone to dielectric breakdown and restrict the separation voltages that can be applied. A dielectric film of adequate thickness (>1 μm) may sustain a relatively high voltage but prevents the anodic bonding of a glass capping, the method of choice for reliably enclosing microchannels in silicon. Here, the glass anodic boding is replaced by a plasma-assisted PDMS bonding which allows a thicker interfacial layer. This
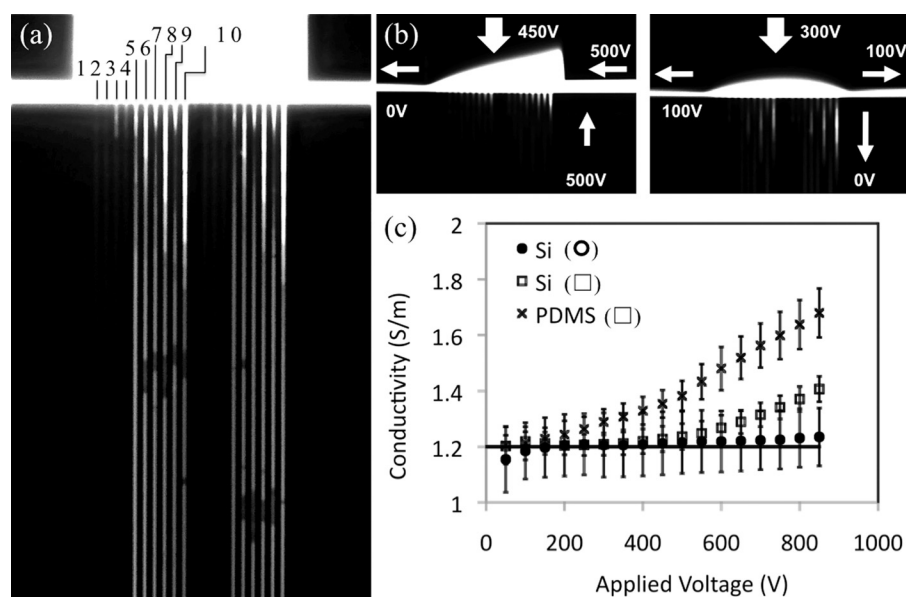
FIG. 4. Fluorescence images of the sample-injection junction: (a) verification of fluidic access to the microcapillaries whereby 5–10 are shown filled with a FITC solution under capillarity, whereas 1–4 could not be filled. The dark segments noticeable on the microcapillaries are probably due to imperfections in the PSG film or the PDMS bonding interface, as they do not interfere with the liquid filling. (b) Electrokinetic sample loading and the formation and injection of sample plugs into the microcapillaries. (c) A plot of conductivity values based on the measurements of current for the voltage intensities applied across the separation channels of a rectangular (□) or round (●) profile.

bonding is required only for enclosing the sample-injection cross; the microcapillaries are self-sealed structures as a result of the non-conformal deposition and thermal reflow of glass. To test for the breakdown voltage, reservoir BW was held at a ground potential while the remaining reservoirs were being subjected to the identical potentials that were stepped up by 50 V increments until a sudden surge of current measured between BW and the ground. This consistently occurred around 900 V for the microcapillaries 10 mm long (three repeats). Although such breakdown voltage appears to be low in consideration of the overall dielectric insulation (a composite of PSG and thermal oxide $>5\,\mu m$ thick), the 10 mm-long microcapillaries could still sustain field strengths adequate for analytical separation (<90 kV/m). This may not be the case for longer microcapillaries as the field strengths they can sustain would decrease proportionally to avoid the fixed breakdown voltage. Thus, experiments here are limited to short (10 mm-long) microcapillaries although much longer microcapillaries (e.g., 70 mm long) have been successfully fabricated through the introduced process. The breakdown failure could be attributed to a relatively thin region (~ 1–$2\,\mu m$ thin) of the dielectric liner on the trench walls surrounding the microcapillaries.

D. Plug injection

Fig. 4(b) presents two representative images of the injection cross immediately before and after switching the voltage protocol from loading to injection. As can be seen, the sample in the injection cross, as it is pumped from reservoir S to SW (right to left), can only be effectively confined (pinched) from one side (reservoir B). This is regardless of the intensity of the voltage applied at reservoir BW because the extremely high resistance of the microcapillaries prevents a strong backflow that can deflect the sample stream. Nevertheless, the voltage applied at BW during the sample loading minimizes sample diffusion into the microcapillaries except for a small fraction of the initial trench segments where the microcapillaries are not fully sealed. This creates a slight offset in the plug size and does not considerably affect the separation. Nevertheless, given the fairly small volume of the microcapillaries, it is important that the injected volume of the sample be minimized to attain reasonably short plugs. This has been

realized by increasing the voltage applied to reservoir B, thereby somewhat pinching the sample stream against the microcapillaries. Further increase in the voltage pins the sample stream before it can reach the junction. Having the sample stream confined to the smallest possible volume within the junction, the voltages are switched to the injection mode with intensities adjusted such that the majority of the sample recedes to reservoirs S and SW (pull back) while only a fraction could get injected into the microcapillaries owing to their high resistance.

E. Joule heating

Thermal performance of the cylindrical glass microcapillaries was investigated by conductivity measurements as the temperature probe.[33] Using the measurement setup and the voltage protocol described above (breakdown experiments), current-voltage characteristics of the microcapillaries were obtained. To overdrive the heating, the microcapillaries were filled with a more concentrated buffer ($\times 10$). For comparison, two device structures, representative of those reported in the literature, were also included in the measurements along with our 10 mm-long microcapillaries. One device underwent the same silicon fabrication process together with our microcapillaries but designed in a way that its separation channel being 30 μm wide could not be sealed at the end of the reflow step. Sealing of the channel was realized by a PDMS cap. Another device was replicated in PDMS and bonded over a glass slide. Both devices posed a channel profile rectangular ($\square$), as opposed to the round ($\bullet$) profile of the glass microcapillaries, with an effective cross-sectional area and SVR accordingly 400 μm^2 and 0.2 μm^{-1} (PDMS) and 138 μm^2 and 0.5 μm^{-1} (Si). In comparison, the effective cross-sectional area and SVR in our device, where 11 out of 20 glass microcapillaries were filled with the buffer, correspond to 25 μm^2 and 2.4 μm^{-1}.

Fig. 4(c) presents a plot of conductivity values based on the measurements of current as a function of the voltage applied. When Joule heating is insignificant, under fairly low voltages, the values from all the three devices converge agreeing more or less with the measurements taken by a conductivity cell at room temperature (1.2 S/m). As the applied voltage is increased, Joule heating can no longer be ignored and the conductivity begins to rise in return. This occurs sooner in the PDMS device at approximately 150 V since it has a cross-sectional area about $\times 3$ and $\times 16$ of the silicon-based devices with rectangular ($\square$) and round ($\bullet$) channel profiles, respectively. The silicon-based devices would proportionally require higher voltages, $\times\sqrt{3}$ and $\times\sqrt{16}$, to generate the same level of heat. In fact, a quick cursory view of the plot confirms this prediction as the conductivity begins to show signs of rise around $\sim$300 V and 600 V for the respective profiles. Despite the fact that they generate a comparable level of heat in comparison to the PDMS device, albeit at higher voltages, a careful comparison of the trends (slopes) suggests that the heating is less severe for the silicon-based devices, in particular for the round microcapillaries. This is because the round microcapillaries can dissipate the generated heat more rapidly as their SVR is nearly $\times 5$ and $\times 12$ of those rectangular channels in silicon and PDMS. Among the rectangular profiles, the one in silicon substrate dissipates heat more readily because of its high-aspect ratio (SVR 0.5 vs. 0.2) as well as the fact that silicon with a thermal conductivity 149 W m^{-1} K^{-1} is far more efficient in transferring heat than glass (1.4 W m^{-1} K^{-1}) and PDMS (0.18 W m^{-1} K^{-1}).[34] All the three devices were bonded with PDMS caps comparable in dimensions. Nevertheless, heat rejection through these caps occurs mainly via convection and thus less effective than the heat rejection through the lower substrates (glass or silicon) via conduction to a room temperature reservoir.[35]

Assuming that the conductivity would increase at a rate of 2%/$^\circ$C, a 40% increase of the conductivity observed with the PDMS device at 850 V suggests a buffer temperature of 45 $^\circ$C. This value is within the range reported by Erickson *et al.* based on the 3D numerical simulations and micro-thermometry measurements of the PDMS-glass microdevices.[35] For the silicon-based devices at 850 V, a conductivity increase of 17.2% through the rectangular channel and a negligible rise ($\sim$1%) through the round microcapillaries suggest a buffer temperature of 34 $^\circ$C and 26 $^\circ$C, respectively. Maintaining only few degrees Celsius above the room temperature while achieving high field strengths is a result of not only effective heat dissipation through the

microcapillaries but also fairly low power dissipation per unit length ($0.22\,\text{W m}^{-1}$) as their high resistance limits the current flow ($2.6\,\mu\text{A}$) for the applied voltage. In comparison, the rectangular channels draw a larger current, $17\,\mu\text{A}$ (silicon) and $57\,\mu\text{A}$ (PDMS), and thus dissipate more power per unit length in the form of heat, $1.5\,\text{W m}^{-1}$ (silicon) and $4.9\,\text{W m}^{-1}$ (PDMS). These values exceed $1\,\text{W m}^{-1}$ reported for the un-cooled conventional fused silica capillaries.[36]

It is also worthwhile to mention that Joule heating is a regenerative positive feedback process: the increased conductivity draws a higher current which then leads to a further increase in the conductivity through Joule heating.[37] Rapid dissipation of heat may break this cycle and stabilize the buffer temperature quickly. In fact, this has been witnessed in the experiments concerning Fig. 4(c). For each increment of 50 V applied, the rising of current to a steady value took about 2 minutes for the PDMS device as opposed to tens of seconds for the round microcapillaries.

F. Electrophoretic separation

The microcapillaries have been characterized for their performance in separating biomolecules. A mixture of FITC-labeled three amino acid molecules (Ser, Gly, and Gln) was loaded into a representative device in which five out of ten microcapillaries (6–10) were filled with the running buffer. Their electropherograms obtained at the detection point (1 mm from reservoir BW) are shown along with a fluorescence image of the microcapillaries in Fig 5(a). Compared with those obtained from the devices with a rectangular profile described earlier and presented in Figs. 5(b) and 5(c), the peaks in the round microcapillaries can be resolved with relative ease as the average resolution for either of the adjacent peaks (Gln-Gly or Gly-Ser) exceeds 1 ($\sim$1.2). In contrast, the resolutions in Figs. 5(b) and 5(c) are rather poor and less than 1 ($\sim$0.8). These values can be enhanced by lowering the amino acid concentrations in the sample plugs. The amino acids had to be applied at fairly high concentrations to overcome the limit of detection imposed by the system and the extremely short optic path across the submicron microcapillaries. Otherwise, a 100-fold dilution would have been recommended for the prepared sample as prescribed in the previous protocols.[4,38,39] Such high sample concentration might have caused electrodispersion, the band broadening under non-uniform field distribution due to mismatched conductivities between the sample zone and the background buffer. Despite the possible occurrence of electrodispersion, the theoretical plate numbers obtained for the peaks here (Table II) are comparable to those reported in the literature.[4,38,39] They range between 6.5×10^3 (Ser) and 11.6×10^3 (Gln) for the round microcapillaries and yet remain below 5×10^3 for more traditional counterparts (except for Gly). The migration times through the
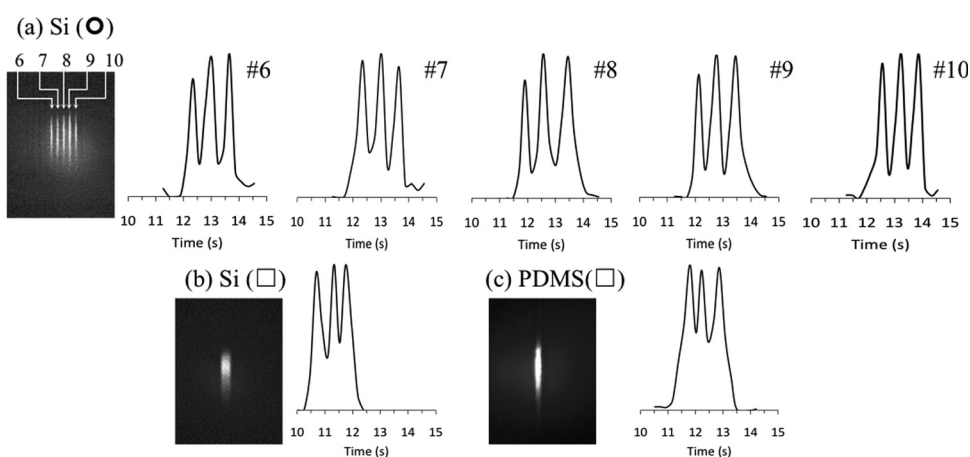

FIG. 5. Representative fluorescent images and electropherograms obtained (a) from round microcapillaries and (b) and (c) from rectangular microchannels during the analyses of a mixture of FITC-labeled three amino acids under the comparable separation field strengths: (a) 281 V/cm, (b) 315 V/cm, and (c) 285 V/cm. The peaks correspond to amino acids Gln, Gly, and Ser according to the order of their migration time (from fast to slow).

TABLE II. Mean theoretical plate number and percent relative standard deviation (RSD %) for the respective bands obtained from five repetitious runs on the Si- and PDMS-based devices with rectangular (□) and round (●) channel profiles.

	Theoretical plate number $\times 10^3$			RSD (%) Migration time			Peak height			Peak area		
	Gln	Gly	Ser	Gln	Gly	Ser	Gln	Gly	Ser	Gln	Gly	Ser
PDMS	2.4	9.1	3.8	0.8	0.8	0.8	8.6	8.7	9.2	5.2	17.1	8.3
Si (□)	3.7	7.0	4.4	4.0	3.9	3.5	5.6	13.9	10.5	10.9	22.8	17.4
Si (●)[a]	9.0	7.7	9.0	2.0	1.9	1.2	12.8	13.7	10.3	19.1	15.1	34.4
Si (●)[b]	11.6	7.6	6.5	2.3	2.2	2.2	16.8	18.0	13.6	17.3	18.8	24.3

[a]The repeats refer to the electropherograms of the separate microcapillaries from the same device in Fig. 5(a).
[b]All the repeats are from the same microcapillary (9).

round microcapillaries are slightly larger averaging at 12.3 s, 12.9 s, and 13.6 s for the peaks FITC-Gln, FITC-Gly, and FITC-Ser, respectively.

Repeatability of the separation was also investigated. Apart from the parallel runs through the adjacent microcapillaries, five repetitious runs were performed on each of the three devices while subjecting them to the same sample mixture and the same field conditions as detailed above. After each run, the devices were cleaned by rinsing the microcapillaries and channels with the running buffer. They were then prepared for a new run with a fresh sample. From the electropherograms, percent relative standard deviation (RSD %) values were calculated for each peak regarding the migration times, peak heights, and peak areas (Table II). The deviations with the Si-based devices were found to be relatively large as compared to those with the PDMS counterpart. This could be partly due to possible deviation in the location of the detection point. The repetitious runs for the PDMS device were performed in one session without disturbing the optical setup, whereas the runs for the Si-based devices were collected in multiple sessions after realigning the optics [except those from Fig. 5(a)]. Furthermore, it must be noted that the optical path length through the Si-based devices is considerably small in comparison to the path length through the PDMS device by a fraction of nearly 20% for the rectangular microchannel and 5% for the round microcapillaries. The signal intensity from such a small volume of molecules may deviate largely and could contribute to the reduced repeatability.

Lastly, our fabrication process differs from the well-known surface micromachining approaches in that it does not ask for etching a sacrificial layer to release thin-film microcapillaries. These known approaches have been utilized to demonstrate molecular devices including μCE.[39,40] However, they typically take long hours of etching to clear a sacrificial layer and thus require a higher etch selectivity against the structural layers. Additionally, thin-film structures are more fragile and vulnerable to damage. They may collapse or break under stresses either intrinsic (residual) or extrinsic related to the process and/or package.

IV. CONCLUSIONS

We have demonstrated monolithic integration of cylindrical glass microcapillaries on silicon and evaluated their performance for the electrophoretic separation of biomolecules. The process takes advantage of the thermal reflow of glass on structured silicon and transforms slender voids buried within the glass layer into cylindrical tubes. The process is highly repeatable and yields microcapillaries with a small diameter ($\sim 1\,\mu$m) uniformly maintained over their entire length (>10 mm). Also disclosed is a simple method of forming access ports to the microcapillaries without the requirement of cumbersome dry etching glass. This method requires a dual-step substrate profile structured with a specific layout to prevent the microcapillary ends from sealing entirely upon the subsequent deposition and reflow of glass. The microcapillaries under the operating field intensities are shown to accumulate less heat with the running buffer temperature rising above the ambient few degrees Celsius only. The microcapillaries achieve this by consuming less power and removing heat more readily all owing to their

high resistance, large SVR, and intimate contact with silicon, an excellent substrate in conducting heat. In return, the round microcapillaries can achieve higher resolutions in the separation of three amino acids as compared to the performance of more traditional μCE devices under comparable field intensities. We are currently extending our work towards the utilization of these microcapillaries for analyzing chemical content of individual cells (chemical cytometry).[41]

ACKNOWLEDGMENTS

[1] D. J. Harrison, A. Manz, Z. H. Fan, H. Ludi, and H. M. Widmer, Anal. Chem. **64**, 1926 (1992).
[2] G. J. M. Bruin, Electrophoresis **21**, 3931 (2000).
[3] S. C. Jacobson, R. Hergenroder, L. B. Koutny, R. J. Warmack, and J. M. Ramsey, Anal. Chem. **66**, 1107 (1994).
[4] C. S. Effenhauser, A. Manz, and H. M. Widmer, Anal. Chem. **65**, 2637 (1993).
[5] J. P. Kutter, S. C. Jacobson, N. Matsubara, and J. M. Ramsey, Anal. Chem. **70**, 3291 (1998).
[6] C. G. Koh, W. Tan, M. Q. Zhao, A. J. Ricco, and Z. H. Fan, Anal. Chem. **75**, 4591 (2003).
[7] K. A. Mahabadi, I. Rodriguez, C. Y. Lim, D. K. Maurya, P. C. Hauser, and N. F. de Rooij, Electrophoresis **31**, 1063 (2010).
[8] A. Floris, S. Staal, S. Lenk, E. Staijen, D. Kohlheyer, J. Eijkel, and A. van den Berg, Lab Chip **10**, 1799 (2010).
[9] N. J. Petersen, R. P. H. Nikolajsen, K. B. Mogensen, and J. P. Kutter, Electrophoresis **25**, 253 (2004).
[10] K. Swinney and D. J. Bornhop, Electrophoresis **23**, 613 (2002).
[11] Y. H. Chen and S. H. Chen, Electrophoresis **21**, 165 (2000).
[12] Y. Zhang, N. Bao, X. D. Yu, J. J. Xu, and H. Y. J. Chen, J. Chromatogr. A **1057**, 247 (2004).
[13] Y. Sun, Y. C. Kwok, and N. T. Nguyen, Electrophoresis **28**, 4765 (2007); Anal. Bioanal. Chem. **394**, 1707 (2009).
[14] S. Ghosal, Anal. Chem. **74**, 771 (2002).
[15] Y. Xu and H. J. E. Wang, Electrophoresis **28**, 4597 (2007).
[16] A. R. Abate, D. Lee, T. Do, C. Holtze, and D. A. Weitz, Lab Chip **8**, 516 (2008).
[17] I. T. Martin, B. Dressen, M. Boggs, Y. Liu, C. S. Henry, and E. R. Fisher, Plasma Processes Polym. **4**, 414 (2007).
[18] I. K. Dimov, A. Riaz, J. Ducrée, and L. P. Lee, Lab Chip **10**, 1468 (2010).
[19] Y. C. Chan, M. Carles, N. J. Sucher, M. Wong, and Y. Zohar, J. Micromech. Microeng. **13**, 914 (2003).
[20] Z. H. Fan and D. J. Harrison, Anal. Chem. **66**, 177 (1994).
[21] S. C. Jacobson, A. W. Moore, and J. M. Ramsey, Anal. Chem. **67**, 2059 (1995).
[22] M. Stjernstrom and J. Roeraade, J. Micromech Microeng. **8**, 33 (1998).
[23] C. Iliescu, J. Miao, and F. E. H. Tay, Sens. Actuators, A **117**, 286 (2005).
[24] X. Li, T. Abe, and M. Esashi, Sens. Actuators, A **87**, 139 (2001).
[25] B. H. Weiller, L. Ceriotti, T. Shibata, D. Rein, M. A. Roberts, J. Lichtenberg, J. Bruce German, N. F. de Rooij, and E. Verpoorte, Anal. Chem. **74**, 1702 (2002).
[26] B. J. Kirby and E. F. Hasselbrink, Jr., Electrophoresis **25**, 187 (2004); **25**, 203 (2004).
[27] M.-S. Kim, S. I. Cho, K.-N. Lee, and Y.-K. Kim, Sens. Actuators, B **107**, 818 (2005).
[28] N. A. Lacher, N. F. de Rooij, E. Verpoorte, and S. M. Lunte, J. Chromatogr. A **1004**, 225 (2003).
[29] A. Agarwal, R. Nagarajan, W. L. Ong, K. C. Tang, and L. Yobas, Sens. Actuators A **142**, 80 (2008).
[30] W. L. Ong, K. C. Tang, A. Agarwal, R. Nagarajan, L. W. Luo, and L. Yobas, Lab Chip **7**, 1357 (2007).
[31] W. L. Ong, J. S. Kee, A. Ajay, R. Nagarajan, K. C. Tang, and L. Yobas, Appl. Phys. Lett. **89**, 093902 (2006).
[32] K. C. Tang, J. Reboud, Y. L. Kwok, S. L. Peng, and L. Yobas, Lab Chip **10**, 1044 (2010).
[33] A. S. Rathore, J. Chromatogr. A **1037**, 431 (2004).
[34] F. P. Incropera and D. P. DeWitt, *Introduction to Heat Transfer* (John Wiley & Sons, New York, 1996).
[35] D. Erickson, D. Sinton, and D. Li, Lab Chip **3**, 141 (2003).
[36] C. A. Monnig and J. W. Jorgenson, Anal. Chem. **63**, 8 (1991).
[37] W. A. Gobie and C. F. Ivory, J. Chromatogr. A **516**, 191 (1990).
[38] J. Su, K. Ren, W. Dai, Y. Zhao, J. Zhou, and H. Wu, Electrophoresis **32**, 3324 (2011).
[39] B. A. Peeni, D. B. Conkey, J. P. Barber, R. T. Kelly, M. L. Lee, A. T. Woolley, and A. R. Hawkins, Lab Chip **5**, 501 (2005).
[40] S. W. Turner, A. M. Perez, A. Lopez, and H. G. Craighead, J. Vac. Sci. Technol. B **16**, 3835 (1998).
[41] H. Wu, A. Wheeler, and R. N. Zare, Proc. Natl. Acad. Sci. U.S.A. **101**, 35, 12809 (2004).